UPTEC F 10067
Examensarbete 30 hp
December 2010

Discontinuous Galerkin Multiscale Methods for Elliptic Problems

Daniel Elfverson

UPPSALA
UNIVERSITET

Teknisk- naturvetenskaplig fakultet
UTH-enheten

Besöksadress:
Ångströmlaboratoriet
Lägerhyddsvägen 1
Hus 4, Plan 0

Postadress:
Box 536
751 21 Uppsala

Telefon:
018 – 471 30 03

Telefax:
018 – 471 30 00

Hemsida:
http://www.teknat.uu.se/student

Abstract

Discontinuous Galerkin Multiscale Methods for Elliptic Problems

Daniel Elfverson

In this paper a continuous Galerkin multiscale method (CGMM) and a discontinuous Galerkin multiscale method (DGMM) are proposed, both based on the variational multiscale method for solving partial differential equations numerically. The solution is decoupled into a coarse and a fine scale contribution, where the fine-scale contribution is computed on patches with localized right hand side. Numerical experiments are presented where exponential decay of the error is observed when increasing the size of the patches for both CGMM and DGMM. DGMM gives much better accuracy when the same size of the patches are used.

Handledare: Axel Målqvist
Ämnesgranskare: Per Lötstedt
Examinator: Tomas Nyberg
ISSN: 1401-5757, UPTEC F 10067

Contents

1 Introduction

In all branches of engineering science there are numerous problems which involve features on several different scales, for example in oil reservoir simulation and organic solar cells. These, so called multiscale problems, are often impossible to solve with standard single mesh methods and therefore require another approach. With a multiscale method the solution is divided into a coarse and a fine scale contribution where the fine scale equation is solved on patches with localized right hand side. The solution to the fine scale equation is then used to solve a modified problem on the coarse scale to obtain the global multiscale solution. In this paper a continuous Galerkin multiscale method, using finite elements (FEM) test spaces, and a discontinuous Galerkin multiscale method, using discontinuous Galerkin (DG) test spaces, are proposed. The methods are derived using the Variational Multiscale Methods (VMS) framework but with a symmetric split for the coarse scale equation. Numerical experiments are presented where exponential decay of the error is observed when increasing the patches for both CGMM and DGMM. For the same accuracy approximately one more layer of coarse element in each patch is needed for CGMM compared to DGMM.

1.1 Previous work

Several multiscale methods have been developed during the last two decades. The multiscale finite element method (MsFEM) was presented by Hou and Wu in [8] and was further developed in [5] where over-sampling was introduced in the patches to reduce the boundary effects. Another approach for solving multiscale problems is VMS, see [9, 10]. The idea is to decompose the problem into one coarse and one fine-scale contribution. The coarse-scale problem is then solved using modified basis functions where the fine-scale contribution has been taken into account. The Adaptive Variational Multiscale Method, (AVMS) using the VMS framework, was introduced by Larson and Målqvist in [11]. A posteriori error estimate in energy norm, where the error is bound in terms of coarse and fine mesh size for the AVMS, was also introduced in [11].

The development of discontinuous Galerkin (DG) methods started in the early seventies and have recently received renewed interests in the last few years. Interior penalty methods are an example of DG methods [6]. They arose from the observation that Dirichlet boundary conditions can be imposed weakly instead of being built in the finite element space, so the inter-element continuity is attained in a similar fashion. Moreover, DG methods are, or are close to locally conservative which is a desired property for example for flow in porous media. The bilinear form for elliptic problems for the Symmetric Interior Penalty Galerkin was first introduced by Wheeler in [13]. A unified analysis for different DG methods for elliptic problems can be found in [3]. A new class of discontinuous Galerkin methods for solving multiscale problems using the MsFEM framework was introduced in [1].

1.2 New contributions

In this paper CGMM which was introduced in [11] and DGMM which has not appeared in literature before, are investigated. Exponential decay for the basis functions are shown experimentally. For the same size of the patches DGMM gives much better accuracy than CGMM, and CGMM needs about one more layer of coarse elements in the localized patches to get the same accuracy.

2 Background

2.1 Preliminaries

For a domain $\omega \subseteq \Omega \subset \mathbf{R}^d$, $d = 1, 2, 3$, with polygonal boundary $\partial\omega$ where $\mathbf{n}$ is the outgoing normal, let $H^k(\omega)$ be a Sobolev space with the corresponding norm $\|u\|^2_{H^k(\omega)} = \sum_{i=1}^{k} \int_\omega |u| + |D^{(i)}u|^2 \, dx$ and $L^p(\omega)$ be a L^p-space with norm $\|u\|^p_{L^p(\omega)} = \int_\omega |u|^p \, dx$, let also $|\omega|$ be the Lebesgue measure of ω. The $L^2(\omega)$ scalar product is $(u, v)_{L^2(\omega)} = \int_\omega uv \, dx$, for simplicity it is written as $(u, v)_{L^2(\omega)} = (u, v)_\omega$, or if $\omega = \Omega$ simply as $(u, v)_{L^2(\Omega)} = (u, v)$. Let us also introduce the space $L^\infty(\omega) = \{v : |v(x)| < \infty \text{ a.e., } x \in \omega\}$. If the domain is left out when defining the spaces it corresponds to the whole domain Ω i.e. $H^k = H^k(\Omega)$ and $L^p = L^p(\Omega)$. The domain Ω is divided into disjoint sets $\mathcal{K} = \{K\}$ where K is called an element. A set of polynomials of degree p_k on each element $\mathcal{P}_{p_k}(K)$ is introduced. Let us also introduce the broken H^1-norm $|||v|||^2 = \sum_{K\in\mathcal{K}} \|\nabla v\|^2_{L^2(K)} + \|v\|^2_{L^2(\Omega)}$. Further discussion about the Sobolev spaces is found in [2].

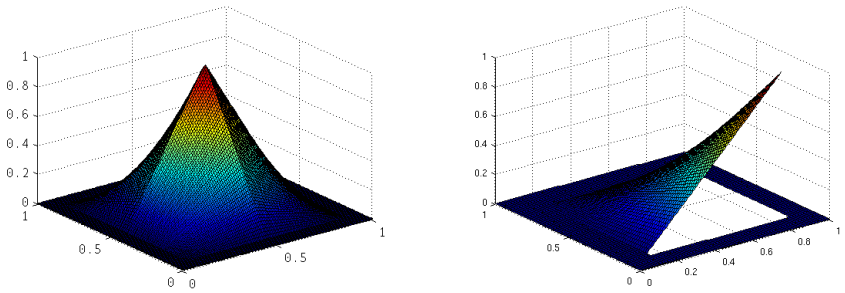

(a) Continuous Galerkin basis function. (b) Discontinuous Galerkin basis function

Figure 1: Example of basis function for FEM (a) and DG (b).

For the finite element method the linear continuous basis function ϕ_i where $\phi_i = 1$ in node i and $\phi_i = 0$ in node $j \neq i$ is used. In the discontinuous Galerkin method the basis function exists only on one element K. Let $\mathcal{M}_i$ consist of all j such that $\phi_j = 1$ in node i and $\mathcal{M}_K$ all j such that $K = supp(\phi_j)$. The basis function ϕ_j is then defined as: ϕ_j is continuous on element K, $\phi_j = 1$ when $j \in \mathcal{M}_i$, $\phi_j = 0$ when $j \in (\mathcal{M}_K \setminus \mathcal{M}_i)$ and $\phi_j = 0$ everywhere else in $\Omega \setminus K$. The same notations for the basis functions in FEM and DG are used, which one we refer to is given by the context.

2.2 The model problem

Given a polygonal domain $\Omega \subset \mathbf{R}^d$, $d = 1, 2, 3$, the Poisson equation with variable coefficients and homogeneous Neumann boundary conditions

$$\begin{cases} -\nabla \cdot \alpha \nabla u = f & u \in \Omega, \\ \mathbf{n} \cdot \nabla u = 0 & u \in \partial\Omega, \end{cases} \tag{1}$$

is studied. Equation (1) has a unique solution $u \in H^1(\Omega)$ up to a constant for each $f \in L^2(\Omega)$ and $\alpha \in L^\infty(\Omega)$ such that $\alpha(x) > \beta > 0$, $\forall x \in \Omega$, provided that $\int_\Omega f\, dx = 0$ is satisfied. Let $\mathcal{V}$ be the space of test functions on Ω, $\alpha : \mathcal{V} \times \mathcal{V} \to \mathbf{R}$ be a bilinear form corresponding to the diffusion operator $-\nabla \cdot \alpha \nabla$ and $l : \mathcal{V} \to \mathbf{R}$ a linear functional corresponding to the forcing function f, the weak formulation of (1) reads: find $u \in \mathcal{V} = H^1(\Omega)$ such that

$$a(u, v) = (-\nabla \cdot \alpha \nabla u, v) = (f, v) = l(v), \quad \forall v \in \mathcal{V}. \tag{2}$$

2.3 The Finite element method

Let the test space be $\mathcal{V} = H^1(\Omega)$. By multiplying (1) with $v \in \mathcal{V}$ and applying Green's formula we arrive at the the weak formulation: find $u \in \mathcal{V} = H^1(\Omega)$ such that

$$a_{cg}(u, v) = (\alpha \nabla u, \nabla v) = (f, v) = l(v), \quad \forall v \in \mathcal{V}. \tag{3}$$

The finite element problem reads: find $U \in \mathcal{V}^{cg} = \{v \in \mathcal{C}(\Omega) : v|_K \in \mathcal{P}_{p_k}(K),\ \forall K \in \mathcal{K}\}$ such that

$$a_{cg}(U, v) = l(v), \quad \forall v \in \mathcal{V}^{cg}. \tag{4}$$

Let $\phi_i \in \mathcal{V}_h$ be one in node i and zero in all nodes $j \neq i$ such that $V_h = span(\phi_i)_{i \in \mathcal{N}}$ where $\mathcal{N}$ is the number of nodes. Write $U = \sum_{i \in \mathcal{N}} \xi \phi_i$, $A_{ij} = a(\phi_i, \phi_j)$ and $b_i = l(\phi_i)$, then equation (4) is transformed to the algebraic expression

$$A\xi = b, \tag{5}$$

which can easily be solved on a computer since A is symmetric and positive definite. The FEM is analyzed in e.g. [4] and convergence is proved.

2.4 The Discontinuous Galerkin method

Let $\Gamma = \cup_{K \in \mathcal{K}} \partial K$ denote the union of all sides of the elements, Γ is the union of two disjoint subsets $\Gamma = \Gamma_{\partial\Omega} \cup \Gamma_{int}$ where $\Gamma_{\partial\Omega} = \partial\Omega \cap \cup_{K \in \mathcal{K}} \partial K$ denotes the union of all boundary sides and $\Gamma_{int} = \cup_{K \in \mathcal{K}} \partial K \backslash \partial\Omega$ the union of all the interior edges. Let us start with some definitions:

Definition 1. *We let $\{v\}$ and $[v]$ be defined by:*

$$\{v\} := \begin{cases} (v^+ + v^-)/2 & v \in \Gamma_{int}, \\ v^+ & v \in \Gamma_{\partial\Omega}, \end{cases} \tag{6}$$

$$[v] := \begin{cases} v^+ - v^- & v \in \Gamma_{int}, \\ v^+ & v \in \Gamma_{\partial\Omega}, \end{cases} \tag{7}$$

where $v^\pm = \lim_{s \to 0^+} v(x \mp s\mathbf{n}_K)$.

Let the discontinuous finite element space be defined by $\mathcal{V}^{dg} = \{v \in L^2(\Omega) : v|_K \in \mathcal{P}_{p_k}(K),\ \forall K \in \mathcal{K})\}$, multiply (1) by $v \in \mathcal{V}$ and apply Green's formula. For element K we arrive at the the weak formulation

$$(\alpha\nabla u, \nabla v)_K = (f, v)_K + (\alpha\nabla u \cdot \mathbf{n}_K, v)_{\partial K}, \tag{8}$$

summing over all element $K \in \mathcal{K}$ and using $a\nabla u \cdot \mathbf{n} = \{a\nabla u \cdot \mathbf{n}\}$ a.e we have

$$\sum_{K\in\mathcal{K}} (\alpha\nabla u, \nabla v)_K = (f, v) + \sum_{e\in\Gamma_{int}} (\{\alpha\nabla u \cdot \mathbf{n}_e\}, [v])_e, \tag{9}$$

where e is an edge in 2–D and a face in 3–D. To arrive at the weak formulation two more terms are added, one for symmetry and one penalty term to make the weak form coercive

$$\begin{aligned} a_{dg}(u, v) = &\sum_{K\in\mathcal{K}} (\alpha\nabla u, \nabla v)_K - \sum_{e\in\Gamma_{int}} (\{\alpha\nabla u\} \cdot \mathbf{n}_e, [v])_e - \sum_{e\in\Gamma_{int}} (\{\alpha\nabla v\} \cdot \mathbf{n}_e, [u])_e \\ &+ \sum_{e\in\Gamma_{int}} \frac{\sigma_e}{|e|}([u], [v])_e, \end{aligned} \tag{10}$$

$$l(v) = (f, v), \tag{11}$$

where $\sigma_e \in \mathbf{R}$ is chosen to be a large enough arbitrary constant. The discontinuous Galerkin method reads: Find $U \in \mathcal{V}^{dg}$ such that

$$a_{dg}(U, v) = l(v) \quad \forall v \in \mathcal{V}^{dg}. \tag{12}$$

Equation (12) is transformed to an algebraic expression in an analogous way as for the continuous case. The DG is analyzed in e.g [3] and references within and convergence is proved.

An important property with this DG method is that it is close to be locally mass conservative i.e. the deviation is computable. To be locally mass conservative means that flow over the boundary should be the same as the created or destroyed mass in each element $K \in \mathcal{K}$ for the approximated solution U in (12) i.e.

$$(\{\alpha \cdot \nabla U\} \cdot \mathbf{n}_e, 1)_{\partial K} = -(f, 1)_K, \tag{13}$$

needs to be satisfied for each $K \in \mathcal{K}$. In (13) the term $(\{\alpha \cdot \nabla U\} \cdot \mathbf{n}_e, 1)_{\partial K}$ corresponds to the flux over the boundary of K and $(f, 1)_K$ the created or destroyed mass in K. Let $w \in \mathcal{V}^{dg}$ be one on element K and zero otherwise, we have

$$\begin{aligned} (\{\alpha \cdot \nabla U\} \cdot \mathbf{n}_e, 1)_{\partial K} &= -(\alpha \cdot \nabla U, \nabla 1)_K + (\{\alpha \cdot \nabla U\} \cdot \mathbf{n}_e, 1)_{\partial K} \\ &\quad + (\{\alpha \cdot \nabla 1\} \cdot \mathbf{n}_e, [U])_{\partial K} - \sum_{e\in\partial K} \frac{\sigma_e}{|e|}([U], 1)_e \\ &\quad + \sum_{e\in\partial K} \frac{\sigma_e}{|e|}([U], 1)_e \qquad (14) \\ &= -a_{dg}(U, w) + \sum_{e\in\partial K} \frac{\sigma_e}{|e|}([U], 1)_e \qquad (15) \\ &= -(f, 1)_K + \sum_{e\in\partial K} \frac{\sigma_e}{|e|}([U], 1)_e, \qquad (16) \end{aligned}$$

where equation (10) and $a_{dg}(U,w) = l(w) = (f,w) = (f,1)_K$ are used. This means that the method is mass conservative if the penalty parameter $\sigma_e = 0$, for standard choices of σ_e the penalty term is typically small and computable. This means that the method is close to be mass conservative and that the deviation can be computed and if necessary be subtracted from the final result. A completely mass conservative method can be obtained by using a non-symmetric DG method.

3 Multiscale Methods

Using the VMS framework, $\mathcal{V}$ is decoupled into a coarse and a fine scale contribution $\mathcal{V} = \mathcal{V}_c \oplus \mathcal{V}_f$, where $\mathcal{V}_c$ is associated with a coarse mesh $\mathcal{K}_c$. We introduce the inclusion operator $\mathcal{I}_c : \mathcal{V} \to \mathcal{V}_c$. The split between the coarse and the fine scale is defined as $\mathcal{V}_c = \mathcal{I}_c\mathcal{V}$ and $\mathcal{V}_f = (I - \mathcal{I}_c)\mathcal{V} = \{v \in \mathcal{V} : \mathcal{I}_c v = 0\}$. Expand $u = u_c + \mathcal{T}u_c + u_f$ and $v = v_c + \mathcal{T}v_c + v_f$ in (1). Here $\mathcal{T}$ is a multiscale projection $\mathcal{T} : \mathcal{V}_c \to \mathcal{V}_f$ defined below in (21) and $u_c, v_c \in \mathcal{V}_c$, $u_f, v_f \in \mathcal{V}_f$. The multiscale problem reads: find $u_c \in \mathcal{V}_c$ and $v_f \in \mathcal{V}_f$ such that

$$a(u_c + \mathcal{T}u_c + u_f, v_c + \mathcal{T}v_c + v_f) = l(v_c + \mathcal{T}v_c + v_f), \quad \forall v_c \in \mathcal{V}_c,\ \forall v_f \in \mathcal{V}_f. \tag{17}$$

A symmetric split proposed in [12] by Målqvist is used. The fine-scale equations are derived be letting $v_c = 0$ in (17): Find $\mathcal{T}v_c \in \mathcal{V}_f$ and $v_f \in \mathcal{V}_f$ such that

$$a(\mathcal{T}u_c + u_c, v_f) = l(v_f) - a(u_c, v_f), \quad \forall v_f \in \mathcal{V}_f, \tag{18}$$

$$a(u_f, v_f) = l(v_f), \quad \forall v_f \in \mathcal{V}_f, \tag{19}$$

$$a(\mathcal{T}u_c, v_f) = -a(u_c, v_f), \quad \forall v_f \in \mathcal{V}_f, \tag{20}$$

where $\mathcal{T}$ is defined by (21) for an arbitrary v_c i.e.

$$a(\mathcal{T}v_c, v_f) = -a(v_c, v_f),\ \forall v_c \in \mathcal{V}_c \text{ and } \forall v_f \in \mathcal{V}_f. \tag{21}$$

The coarse-scale solution is obtained by letting $v_f = 0$ in (17): Find $v_c \in \mathcal{V}_c$ such that

$$a(u_c + \mathcal{T}u_c, v_c + \mathcal{T}v_c) = l(v_c + \mathcal{T}v_c) - a(u_f, v_c + \mathcal{T}v_c), \quad \forall v_c \in \mathcal{V}_c, \tag{22}$$

In (22) $\mathcal{T}v_c$ and v_f are unknown and obtained by solving (19) and (21). Note that $a(u_f, v_c + \mathcal{T}v_c) = 0$ in the continuous case but not when $\mathcal{T}$ is approximated, i.e. calculated on a patch $\omega \subset \Omega$ and not the whole domain Ω. An example what an approximate solution $u = u_f + \mathcal{T}u_c + u_f$ can look like is given in Figure 2.

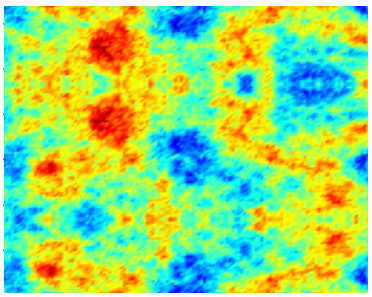

(a) Permeability structure a projected in log scale.

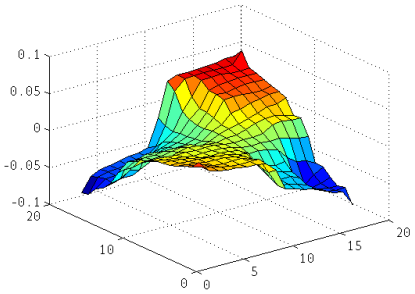

(b) Coarse scale solution, u_c.

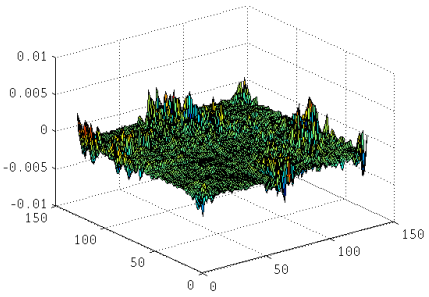

(c) Fine scale correction of the multiscale coefficient a, $\mathcal{T}u_c$.

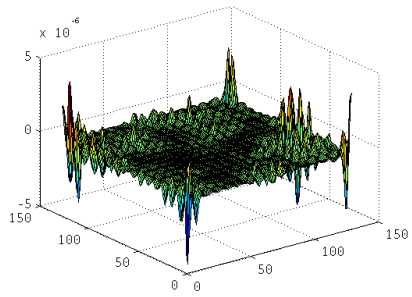

(d) Fine scale correction of the forcing function f, u_f.

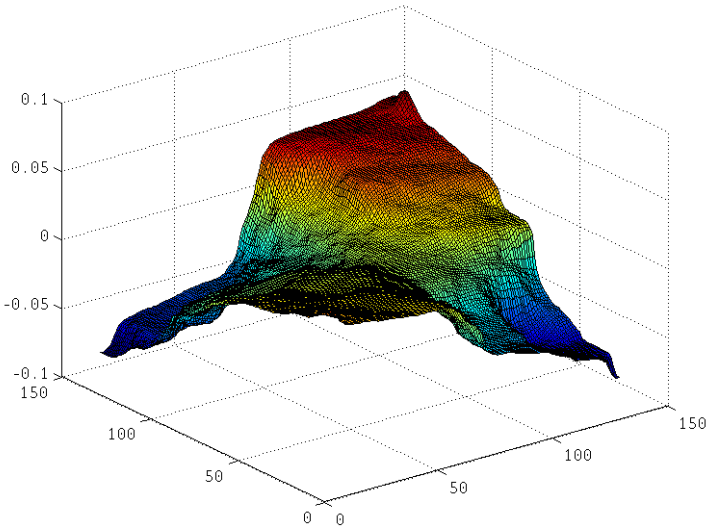

(e) Multiscale solution, $u = u_c + \mathcal{T}u_c + u_f$.

Figure 2: The multiscale solution (e) is obtained from the coarse scale equation (b) using fine scale corrections from the multiscale coefficient (c) and forcing function (d) computed on the domain (a).

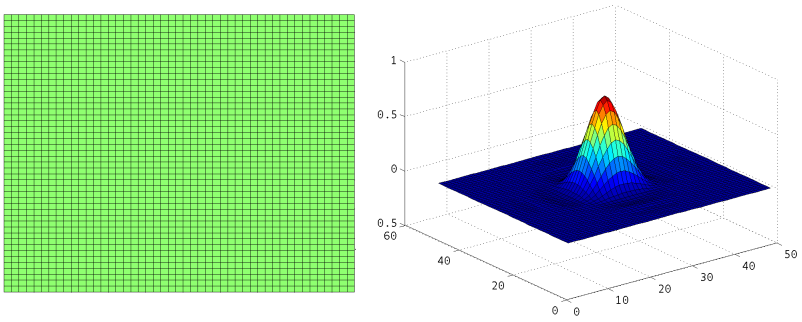

(a) *One*

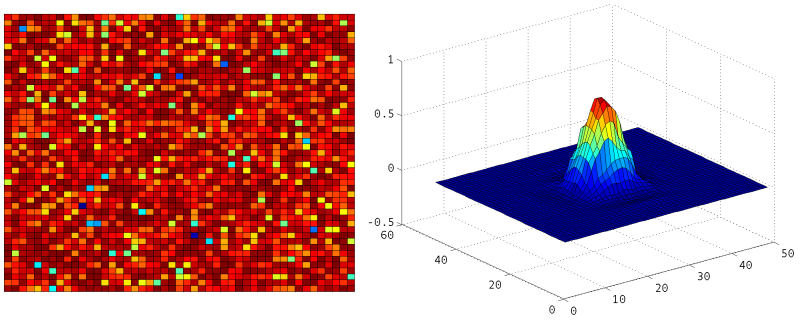

(b) *Rand*

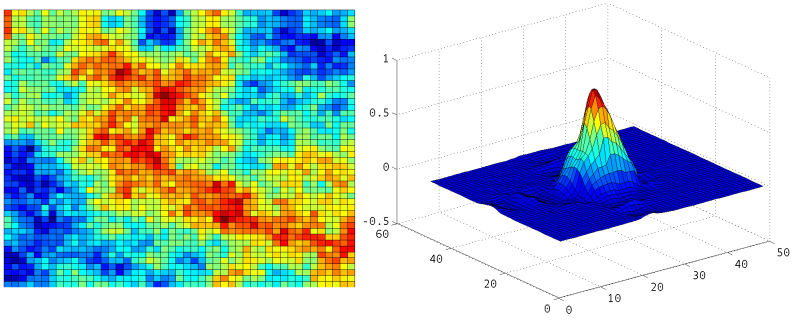

(c) *SPE*

Figure 3: Example of a modified basis functions $\phi_i + \mathcal{T}\phi_i$ computed on a domain ω. Three different multiscale coefficient are used, *One* then a=1, *Rand* then a is a uniformly distributed random numbers between (0, 1] on each element and *SPE* then the data is taken from `http://www.spe.org/web/csp/`.

3.1 Localization and Discretization

Because the bilinear form has a more local behavior in $\mathcal{V}_f$ than in $\mathcal{V}$ as can be seen in Figure 3 the fine-scale equations are solved on small overlapping patches ω_i^L, see Definition 2, to get good approximations of $\mathcal{T}v_c$ and u_f. This can be done in parallel with localized right hand sides.

Definition 2. *ω_i^1 is a 1-layer patch if $\omega_i^1 = supp(\Phi_i)$, where $\Phi_i = \sum_{j\in\mathcal{M}_i}\phi_j$. Here ϕ_j is a coarse basis function and $\mathcal{M}_i$ consists of all j such that $\phi_j = 1$ in node i. Further we say that ω_i^L is a L-layer patch if,*

$$\omega_i^L = \cup_{\{i:supp(\Phi_i)\cap\omega_i^{L-1}\}\neq\emptyset} supp(\Phi_i), \quad L = 2, 3, \ldots \tag{23}$$

For each L we add one more L-ring around node i. This is illustrated in Figure 4

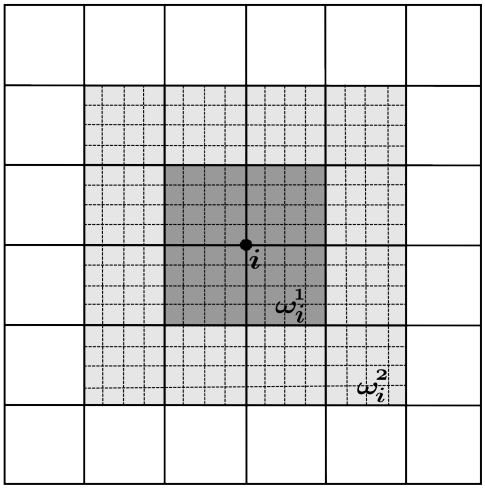

Figure 4: Example of a patch with one L-ring w_i^1 and two L-rings ω_i^2 around node i.

Let us introduce the discrete spaces $\mathcal{V}_c^{cg}$ using FEM for CGMM and $\mathcal{V}_c^{dg}$ using DG for DGMM on the coarse mesh $\mathcal{K}_c = \{K\}$. The domain Ω is the union of coarse elements i.e. $\cup_{K\in\mathcal{K}_c}K = \Omega$, let also $\mathcal{K}_f(\omega_i^L) = \{K \in \mathcal{K} : K \in \omega_i^L\}$ be a local fine mesh for each $i \in 1, \ldots, \mathcal{N}$, where $\omega_i^L \subset \Omega$ is the union of fine elements i.e. $\cup_{K\in\mathcal{K}_f(\omega_i^L)}K = \omega_i^L$. Let us also assume that $\mathcal{K}_c \cap \omega_i^L$ and $\mathcal{K}_f(\omega_i^L)$ are nested so that any $K \in \mathcal{K}_c \cap \omega_i^L$ can be written as a union of elements in $K \in \mathcal{K}_f(\omega_i^L)$. The discrete approximations of $\mathcal{V}_f$ for CGMM are

$$\mathcal{V}_f^{cg}(\omega_i^L) = \{v \in \mathcal{V}^{cg}(\omega) : \mathcal{I}_c v = 0\}, \tag{24}$$

and for DGMM

$$\mathcal{V}_f^{dg}(\omega_i^L) = \{v \in \mathcal{V}^{dg}(\omega) : \mathcal{I}_c v = 0\}. \tag{25}$$

3.2 CGMM

In CGMM the split between the coarse and fine mesh is realized using the nodal interpolant as the inclusion operator $\mathcal{I}_c = \Pi_c$ and the fine-scale equation is solved on patches with a homogeneous Dirichlet boundary condition. Let $\mathcal{N}$ be the number of nodes in the coarse mesh $\mathcal{K}$ and let $\mathcal{V}_c = span\{\phi_i\}_{i\in\mathcal{N}}$. For each $i \in \mathcal{N}$ we need to solve the local problems: Find $\tilde{\mathcal{T}}\phi_i \in \mathcal{V}^{cg}(\omega_i^L)$ and $U_{f,i} \in \mathcal{V}^{cg}(\omega_i^L)$ such that

$$a_{cg}(\tilde{\mathcal{T}}\phi_i, v_f) = -a_{cg}(\phi_i, v_f), \quad \forall v_f \in \mathcal{V}_f^{cg}(\omega_i^L), \tag{26}$$

$$a_{cg}(U_{f,i}, v_f) = l(\phi_i v_f), \quad \forall v_f \in \mathcal{V}_f^{cg}(\omega_i^L), \tag{27}$$

where $U_f = \sum_{i\in\mathcal{N}} U_{f,i}$.

The modified coarse scale problem is formulated as: Find $U_c \in \mathcal{V}_c^{cg}$ such that

$$a_{cg}(U_c + \tilde{\mathcal{T}}U_c, v_c + \tilde{\mathcal{T}}v_c) = l(v_c + \tilde{\mathcal{T}}v_c) - a_{cg}(U_f, v_c + \tilde{\mathcal{T}}v_c), \quad \forall v_c \in \mathcal{V}_c^{cg}. \tag{28}$$

The approximate solution to the multiscale problem is $U = U_c + \tilde{\mathcal{T}}U_c + U_f$.

3.3 DGMM

For DGMM the split is done using the L^2-projection onto the coarse mesh $\mathcal{I}_c = \mathcal{P}_c$, so that $\mathcal{V}_c = \mathcal{P}_c\mathcal{V}$ and $\mathcal{V}_f = (\mathcal{I} - \mathcal{P}_c)\mathcal{V}$. This should be a better choice than the nodal interpolate because the L^2-projection approximates the mean value while the nodal interpolate gives an exact value in the nodes.

The fine-scale equations are solved on patches with homogeneous Neumann boundary condition, which is a more natural choice and can be used because DGMM can handle discontinuities between the basis functions. Let $\mathcal{N}$ be the number of coarse nodes and $\mathcal{M}_i$ contain all j such that ϕ_j is equal to one in node i. For each $i \in \mathcal{N}$ we need to solve the local problems: find $\tilde{\mathcal{T}}\phi_j \in \mathcal{V}_f(\omega_i^L)$, $\forall j \in \mathcal{M}_i$ and $U_{f,i} \in \mathcal{V}_f(\omega_i^L)$ such that

$$a_{dg}(\tilde{\mathcal{T}}\phi_j, v_f) = -a_{dg}(\phi_j, v_f), \quad \forall v_f \in \mathcal{V}_f^{dg}(\omega_i^L), \tag{29}$$

$$a_{dg}(U_{f,i}, v_f) = l(\Phi_i v_f), \quad \forall v_f \in \mathcal{V}_f^{dg}(\omega_i^L), \tag{30}$$

where $\Phi_i = \sum_{j\in\mathcal{M}_i} \phi_j$ and $U_f = \sum_{i\in\mathcal{N}} U_{f,i}$.

The modified coarse scale problem is formulated as: Find $U_c \in \mathcal{V}_c^{dg}$ such that

$$a_{dg}(U_c + \tilde{\mathcal{T}}U_c, v_c + \tilde{\mathcal{T}}v_c) = l(\phi_i + \tilde{\mathcal{T}}v_c) - a_{dg}(U_f, v_c + \tilde{\mathcal{T}}v_c), \quad \forall v_c \in \mathcal{V}_c^{dg}. \tag{31}$$

The approximate solution to the multiscale problem is $U = U_c + \tilde{\mathcal{T}}U_c + U_f$.

An important property of DGMM is that it is close to be locally mass conservative. To be mass conservative means that the approximated solution U for the multiscale problem satisfies

$$(\{\alpha \cdot \nabla U\} \cdot \mathbf{n}_e, 1)_{\partial K} = -(f, 1)_K, \tag{32}$$

for each $K \in \mathcal{K}$. In (32) the term $(\{\alpha \cdot \nabla U\} \cdot \mathbf{n}_e, 1)_{\partial K}$ corresponds to the flux over the boundary of K and $(f, 1)_K$ the created or destroyed mass in K. Let

$w \in \mathcal{V}^{dg}$ be w=1 on element K and $w = 0$ on ∂K we have

$$
\begin{aligned}
(\{\alpha \cdot \nabla U\} \cdot \mathbf{n}_e, 1)_{\partial K} &= (\{\alpha \cdot \nabla U_c\} \cdot \mathbf{n}_e, 1)_{\partial K} + (\{\alpha \cdot \nabla \tilde{\mathcal{T}} U\} \cdot \mathbf{n}_e, 1)_{\partial K} \\
&\quad + (\{\alpha \cdot \nabla U_f\} \cdot \mathbf{n}_e, 1)_{\partial K}) \qquad (33) \\
&= -a_{dg}(U, w) - a_{dg}(\tilde{\mathcal{T}} U, w) - a_{dg}(U_f, w) \\
&\quad + \sum_{e \in \partial K} \frac{\sigma_e}{|e|} \big(([U], 1)_e + ([\tilde{\mathcal{T}} U], 1)_e + ([U_f], 1)_e \big) \qquad (34) \\
&= -a_{dg}(U_f, w) + \sum_{e \in \partial K} \frac{\sigma_e}{|e|} ([U], 1)_e \qquad (35) \\
&= -(f, 1) + \sum_{e \in \partial K} \frac{\sigma_e}{|e|} ([U], 1)_e, \qquad (36)
\end{aligned}
$$

where equation (10) and $a_{dg}(U_f, w) = (f, w) = (f, 1)_K$ are used. The deviation is computable and can if necessary be subtracted from the end result, see Section 2.4 for further analysis.

3.4 Implementation for DGMM

The algorithm used in the implementation is presented in Algorithm 1 and is given an overview in Figure 5. Here $\mathcal{N}$ are the number of nodes in the coarse mesh. The constraints on the fine scale $\mathcal{V}_f = (I - \mathcal{I}_c)\mathcal{V}$ is realized

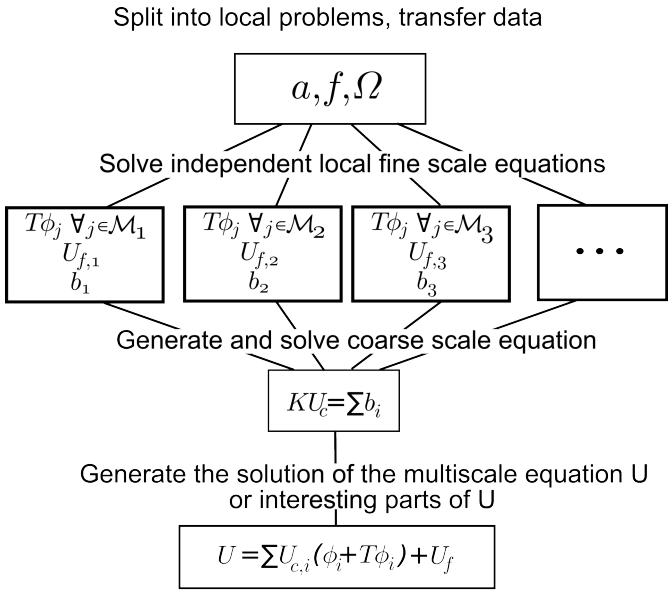

Figure 5: Sketch over the implementation structure for DGMM

using Lagrangian multipliers. The spaces $\mathcal{V}_f$ and $\mathcal{V}_c$ are L^2-orthogonal to each other which means that $(v_c, v_f) = 0$ for all $v_f \in \mathcal{V}_f(\omega)$ and $v_c \in \mathcal{V}_c(\omega)$. Let $\mathcal{V}_c = \text{span}(\phi_i)$ and $\mathcal{V}_f = \text{span}(\varphi_i)$, then the system of equations to be solved on the fine scale is,

$$
\begin{pmatrix} K & P^T \\ P & 0 \end{pmatrix} \xi = \begin{pmatrix} b \\ 0 \end{pmatrix}, \qquad (37)
$$

Algorithm 1 DGMM

1: Initialize the coarse mesh with mesh size h_c.
2: Let the fine mesh size be $h_f = h_c/2^n$ and the number of L-rings be L where n, L are integers greater than 0.
3: **for** $i \in \mathcal{N}$ **do**
4: Determine the patch ω_i^L.
5: Compute $\tilde{\mathcal{T}}\phi_j$ for all $j \in \mathcal{M}_i$ by solving (29)
6: Compute $U_{f,i}$ by solving (30)
7: Compute b_j for all $j \in \mathcal{M}_i$ by solving the right hand side of (31) using $U_{f,i}$ and $\phi_j + \tilde{\mathcal{T}}\phi_j$
8: **end for**
9: Assemble the stiffness matrix K for and solve the modified problem $K\beta = b$ (31) .
10: The approximate solution to the multiscale problem is $U = \sum_j \beta_j(\phi_j + \tilde{\mathcal{T}}\phi_j) + \sum_i U_{f,i}$.

where

$$P = \begin{pmatrix} (\phi_1, \varphi_1) & (\phi_1, \varphi_2) & \dots & (\phi_1, \varphi_N) \\ (\phi_2, \varphi_1) & (\phi_2, \varphi_2) & \dots & (\phi_2, \varphi_N) \\ \vdots & \vdots & \ddots & \vdots \\ (\phi_M, \varphi_1) & (\phi_M, \varphi_2) & \dots & (\phi_M, \varphi_N) \end{pmatrix}. \tag{38}$$

Here K is the stiffness matrix, b is the load vector and $U = \sum_j \xi\varphi_j$ is the solution to (37). For the coarse scale problem the condition $\int_\Omega u \, dx = 0$ is added to get a full rank matrix, this condition is realized using Lagrangian multipliers. All the code was implemented in MATLAB.

3.5 Choice of penalty parameter σ

The penalty parameter σ_e in (10) is chosen as $\sigma_e = C(\frac{(k_1^{K^+})^2}{k_0^{K^+}} + \frac{(k_1^{K^-})^2}{k_0^{K^-}})$ where $k_o^K x^T x \leq x^T \alpha(x) x \leq k_1^K x^T x$, $\forall x \in K$. Here e is the common side of K^+ and K^-. The constraint's is inspired by [7] where they derive a strict C for triangular meshes. In the case of piecewise constant function on each element the penalty parameter is $\sigma_e = C(k^{K^+} + k^{K^-})$ where k^K is the value of α in element K. The same choice of the penalty parameter σ is used both when solving the coarse and fine scale equations.

4 Numerical Results

4.1 Decay of basis functions for CGMM and DGMM

Let the domain be $\Omega = \omega_i^L$ and the forcing function $f = \phi_i - \frac{1}{|\Omega|}\int_\Omega \phi_i$ on ω_i^1 and $f = 0$ otherwise, where $\phi_i \in \mathcal{V}_c$ is a coarse basis function. Let us look at the model problem (1) for $L = 1, 2, \ldots, N$. For each L we add one more layer of L-rings around ϕ_i. The discrete weak formulation of the problem reads: find $u \in \mathcal{W}$ such that,

$$a(u, v) = l(v), \quad \forall v \in \mathcal{W}, \tag{39}$$

where $\mathcal{W} = \{v \in \mathcal{V}^h : \mathcal{P}_c v = 0\}$, here $\mathcal{V}^h = \mathcal{V}^{cg}$ for CGMM and $\mathcal{V}^h = \mathcal{V}^{dg}$ for DGMM. The decay of the L^2-norm on the boundary $\|u\|_{L^2(\partial\Omega)}$ and the

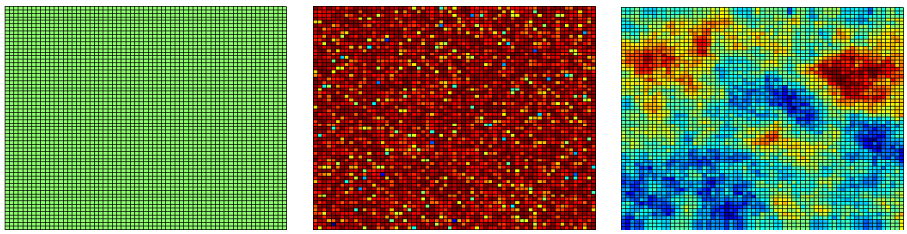

(a) One (b) Rand (c) SPE

Figure 6: Permeability structure for One (a), Rand (b) and SPE (c) projected in log scale.

convergence of the energy norm $|||U_L - U_N|||$ for $L = 1, \ldots, N$ when $N = 4$. A few different multiscale coefficients a with different characters is investigated.

The test was done using the following permeabilities, *One* then a=1, *Rand* then a has uniformly distributed random numbers between $(0, 1]$ and *SPE* data is taken from the tenth SPE comparative solution project and has $a_{max}/a_{min} = 2.3584 \cdot 10^4$. The different permeabilities are shown in Figure 6.

Exponential decay is observed with respect to the number of L-rings for $\|u\|_{L^2(\partial\Omega)}$ of the solution, presented in Figure 7 using $L = 1, 2, 3, 4$. The speed of convergences in the energy norm is shown in Figure 8. Because of the quick decay this means that we can solve the localized fine-scale problems on a subset $\omega_i^L \subset \Omega$ using a small number of L-rings to get a good approximation of the solution, which in turn means less computational work and the overlap between the localized problems will also be less. The DG method converges both faster to U_N in the energy norm and has a faster decay on the boundary. Hence, fewer L-rings are needed for solving the local problems using DG than for CG test spaces to achieve the same accuracy.

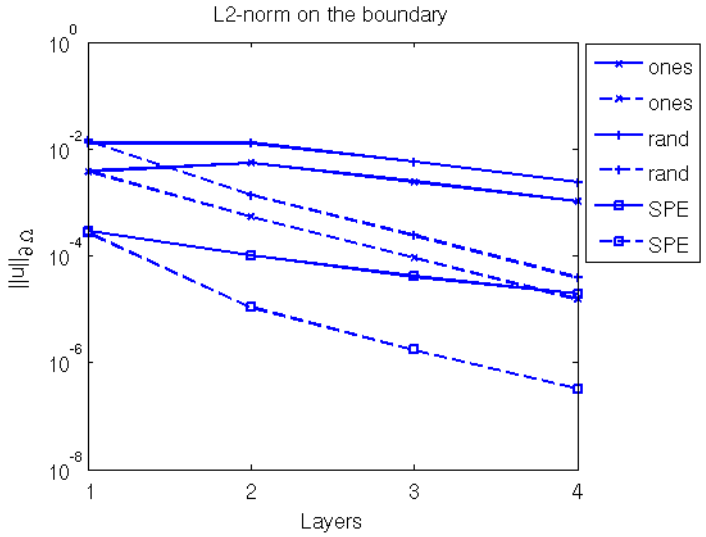

Figure 7: Decay of the solution $\|u\|_{L^2(\partial\Omega)}$ in equation (39) for different permeability using continuous Galerkin (solid line) and discontinuous Galerkin (dashed line) on the space $\mathcal{W} = \{v \in \mathcal{V}^h : \mathcal{P}_c v = 0\}$.

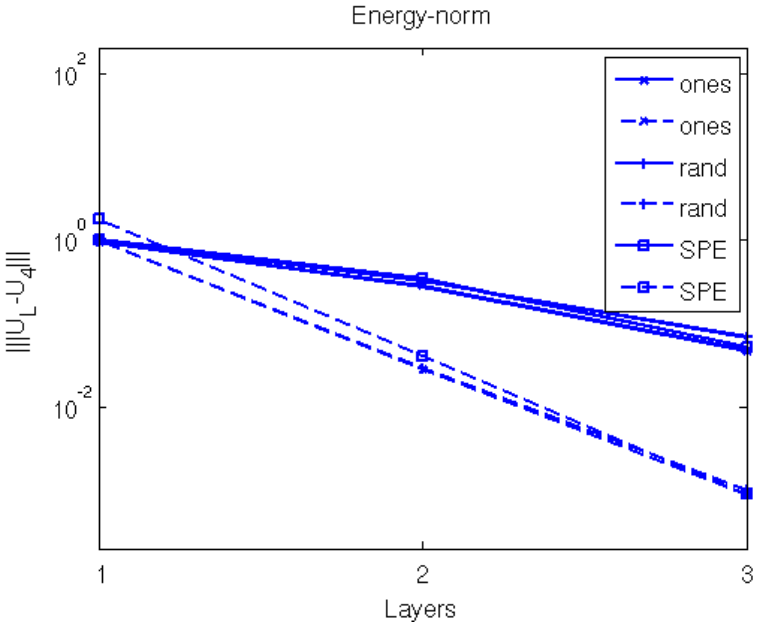

Figure 8: Convergence of $|||U_L - U_4|||$ when $L = 1, 2, 3$ in equation (39) for different permeability using continuous Galerkin (solid line) and discontinuous Galerkin (dashed line) on the space $\mathcal{W} = \{v \in \mathcal{V}^h : \mathcal{P}_c v = 0\}$.

4.2 Convergence of CGMM

Let $\Omega = (0,1) \times (0,1)$ be the computational domain, further let $\mathcal{K} = \{K\}$ be a coarse mesh defined on Ω with $N \times N$ square elements where each element $K \in \mathcal{K}_c$ is further subdivided into $M \times M$ square elements. The model problem (1) is solved using the forcing function

$$f(x,y) = 2\pi^2 \cos(\pi x)\cos(\pi y), \tag{40}$$

and with the different multiscale structures *One*, *Rand* and *SPE*. When the multiscale structure is *One* then a=1, with *Rand* then a is a uniformly distributed pseudo random numbers between (0,1] on each element and with *SPE* the data is taken from the tenth SPE comparative solution data set and shown in Figure 9.

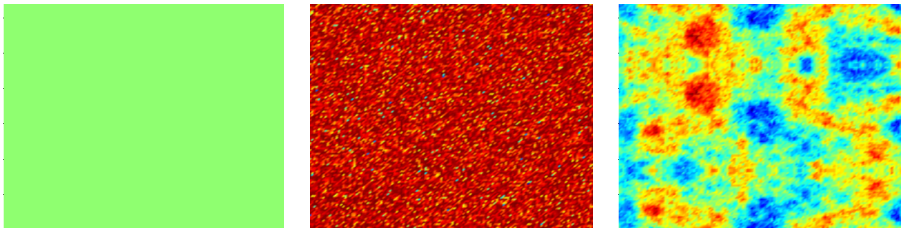

(a) One (b) Rand (c) SPE

Figure 9: Permeability layer from the tenth SPE comparative solution data set projected in log scale.

The convergence is measured in the relative energy norm

$$E(U_L) = \frac{|||U_L - U_r|||}{|||U_r|||}, \tag{41}$$

where U_r is a reference solution computed on a fully resolved mesh with $NM \times NM$ square elements. The numerical test was done using $N = 16$, $M = 8$ and by letting L increase i.e. $L = 1, 2, \ldots, N$ such that $\omega_i^N = \Omega$ for all i. Here U_L is the solution using the computational domain ω_i^L for each patch when solving the fine-scale problems.

In Figure 10 exponential decay is observed for the different permeabilities *One*, *Rand* and *SPE*, with respect to the number of L-rings in the for relative energy norm $E(U_L)$.

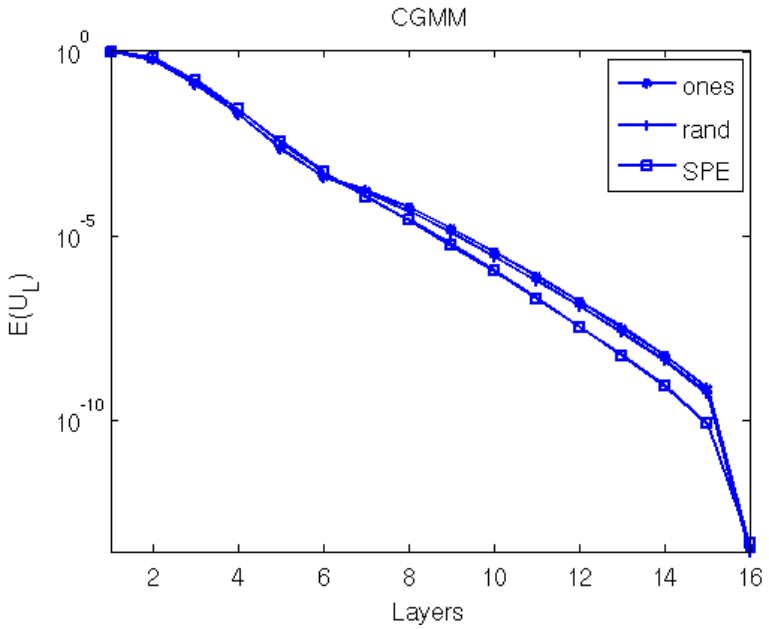

Figure 10: Convergence in the relative energy norm $E(U_L)$, equation (41), when L increases using the different permeabilities *One*, *Rand* and *SPE* for CGMM.

4.3 Convergence of DGMM

Here the same setup as in Section 4.2 is used, The model problem (1) is solved using the permabilities *One*, *Rand* and *Spe* with the forcing function (40) and Ω is split into $N \times N$ coarse square elements where each coarse element $K \in \mathcal{K}_c$ is further subdivided into $M \times M$ fine square elements. The error is measured in the relative energy norm (41).

In Figure 11, exponential decay is observed for the different permeabilities *One*, *Rand* and *SPE*, with respect to the number of L-rings in the relative energy norm $E(U_L)$.

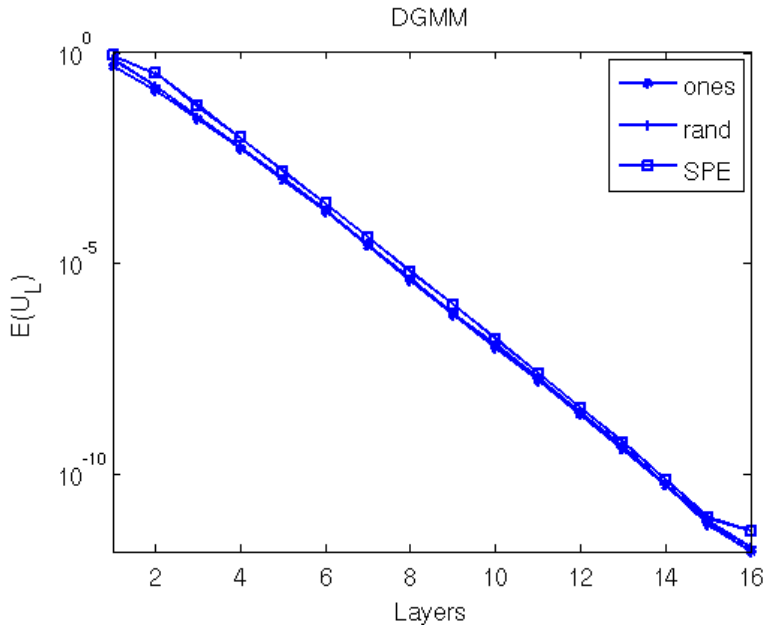

Figure 11: Convergence in relative energy norm $E(U_L)$, equation (41), when L increases using the different permabilities *One*, *Rand* and *SPE* for DGMM.

5 Conclusions

Both CGMM and DGMM has exponential decay when increasing the number of L-rings for the patches. In practice when solving multiscale problem seldom more than a few L-rings are needed to get a sufficient solution. In Figure 12, CGMM and DGMM are compared for the first three layers. In the case of permeability *One* in Figure 12(a) and permeability *Rand* in Figure 12(b), the accuracy are approximately the same for CGMM and DGMM when using one layer less for DGMM. This is not the case when using permeability *SPE* in Figure 12(c) even though the DGMM solution is more accurate for the same number of layers. This could depend on the choice of penalty parameter σ_e. Using a larger σ_e in the case of permeability *One* and *Rand*, the plot of the error for DGMM is approaching the plot of error for CGMM in a similar way as in Figure 12(c). Typically DG gives a better solution for discontinuous data than FEM. This effect can not be seen in our experiments since we compare with FEM and DG as reference solutions.

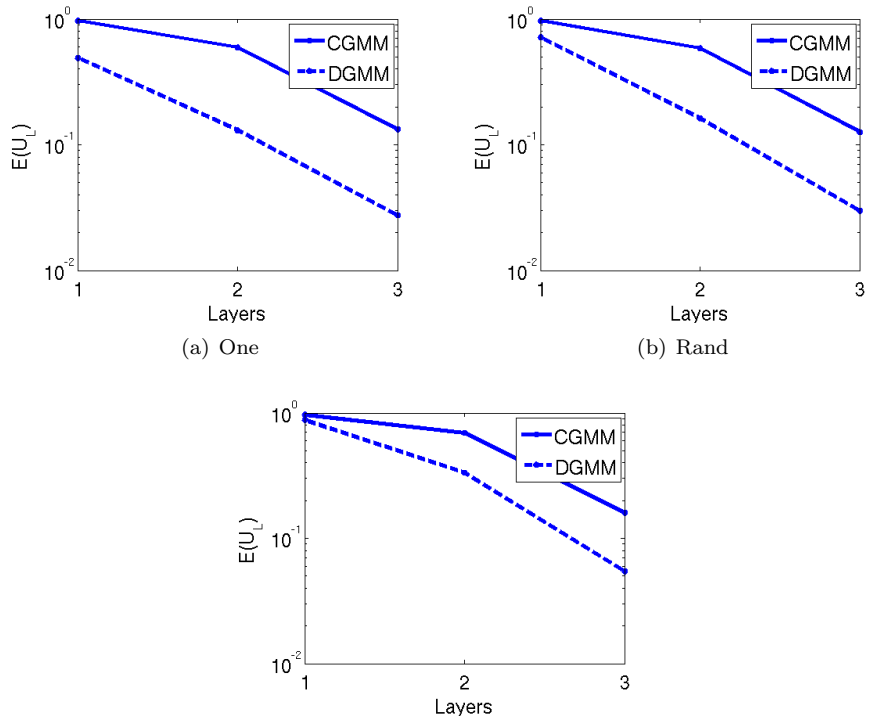

(a) One (b) Rand

(c) SPE

Figure 12: Comparing the relative energy norm $E(U_L)$ for CGMM and DGMM on the first three layers using the different permeabilities *One* (a), *Rand* (b) and *SPE* (c)

The degrees of freedom for solving fine-scale problem is $(n(2L-1)+1)^d$ for CGMM and $(2n(2L-1))^d$ for DGMM. Here n is the number of elements for each spatial direction for a one layer patch and d the is the spatial dimension. Let us say that the acquired accuracy is obtained by using two layers for CGMM and one layers for DGMM. Then each fine-scale problem has $(3n+1)^d$ degrees of freedom when using CGMM and $(2n)^d$ degrees of freedom when using DGMM, which means that in this case it takes less computational work to solve each fine scale equation and the overlap between the localized problems will also be less, see Table 1. DGMM also has the desired property that it is close to be

Table 1: Let n be the number of elements for each spatial direction for a one layer patch in the mesh. This shows the degree of freedom for the fine scale problems using a different number of L-rings. Without parenthesis is the amount of layers for CGMM and with parenthesis is for DGMM.

layers	CGMM	DGMM
1	$(n+1)^d$	–
2 (1)	$(3n+1)^d$	$(2n)^d$
3 (2)	$(5n+1)^d$	$(6n)^d$
4 (3)	$(7n+1)^d$	$(10n)^d$

locally mass conservative, which is very important property in flow calculations. This means that without using heavier computations we obtain a close to mass conservative more accurate multiscale method. A completely mass conservative method could be obtained by using a non-symmetric DG method.

References

[1] J. Aarnes and B.-O. Heimsund. *Multiscale Discontinuous Galerkin Methods for Elliptic Problems with Multiple Scales*, volume 44 of *Lecture Notes in Computational Science and Engineering*. Springer Berlin Heidelberg, 2005.

[2] R. A. Adams. *Sobolev spaces / Robert A. Adams*. Academic Press, New York :, 1975.

[3] D. Arnold, F. Brezzi, B. Cockburn, and L. Marini. Unified analysis of discontinuous Galerkin methods for elliptic problems. *SIAM J. Numer. Anal.*, 39(5):1749–1779, 2001.

[4] S. C. Brenner and L. R. Scott. *The Mathematical Theory of Finite Element Methods The Mathematical Theory of Finite Element Methods*. Springer Verlag, 1979.

[5] J. Chu, Y. Efendiev, V. Ginting, and T. Y. Hou. Flow based oversampling technique for multiscale finite element methods. *Advances in Water Resources*, 31(4):599 – 608, 2008.

[6] J. Douglas and T. Dupont. *Interior Penalty Procedures for Elliptic and Parabolic Galerkin Methods*, volume 58 of *Lecture Notes in Physics*. Springer Berlin / Heidelberg, 1976. 10.1007/BFb0120591.

[7] Y. Epshteyn and B. Rivière. Estimation of penalty parameters for symmetric interior penalty Galerkin methods. *Journal of Computational and Applied Mathematics*, 206(2):843 – 872, 2007.

[8] T. Y. Hou, T. Y. Hou, and X.-H. Wu. A multiscale finite element method for elliptic problems in composite materials and porous media. *Journal of Computational Physics*, 134:169–189, 1997.

[9] T. Hughes. Multiscale phenomena: Green's functions, the Dirichlet-to-Neumann formulation, subgrid scale models, bubbles and the origins of stabilized methods. *Computer Methods in Applied Mechanics and Engineering*, 127(1-4):387 – 401, 1995.

[10] T. Hughes, G. Feijóo, L. Mazzei, and J.-B. Quincy. The variational multiscale method–a paradigm for computational mechanics. *Computer Methods in Applied Mechanics and Engineering*, 166(1-2):3 – 24, 1998. Advances in Stabilized Methods in Computational Mechanics.

[11] M. G. Larson and A. Målqvist. Adaptive variational multiscale methods based on a posteriori error estimation: Energy norm estimates for elliptic problems. *Computer Methods in Applied Mechanics and Engineering*, 196(21-24):2313 – 2324, 2007.

[12] A. Målqvist. Multiscale methods for elliptic problems. *Submitted*.

[13] M. Wheeler. An elliptic collocation-finite element method with interior penalties. *SIAM Journal on Numerical Analysis*, 15(1):pp. 152–161, 1978.